








Cite this: *J. Anal. At. Spectrom.*, 2025, 40, 848

# Challenges in measuring nanoparticles and microparticles by single particle ICP-QMS and ICP-TOFMS: size-dependent transport efficiency and limited linear dynamic range†

Madeleine Lomax-Vogt, <sup>ab</sup> Lucas M. Carter, <sup>a</sup> Jonas Wielinski, <sup>d</sup> Stanislav Kutuzov, <sup>ac</sup> Gregory V. Lowry, <sup>d</sup> Ryan Sullivan, <sup>e</sup> Paolo Gabrielli<sup>f</sup> and John W. Olesik <sup>\*ac</sup>

While spICP-MS has been used mainly to measure nanoparticles, it can also be used to measure microparticles. The transport efficiency of nanoparticles is typically independent of their size. However, the transport efficiency of microparticles can be particle size (mass) dependent as well as being dependent on the sample uptake rate and sample introduction system used. To measure both nanoparticles and microparticles a very large linear dynamic range (where signal intensity is linearly proportional to the measured analyte(s) mass within a very short measurement time (~300 to 500  $\mu$ s, the width of signals produced by an individual particle)) is needed. Deviations from linearity could occur due to incomplete particle vaporization or from signals that are beyond the instrument's ion detection system linear dynamic range. To characterize and determine the cause of nonlinearity we measured sets of nearly monodisperse engineered SiO<sub>2</sub> particles with diameters from 500 to 5000 nm and Au particles with diameters from 60 to 1500 nm. We found that by reducing the sensitivity (up to a factor of 269 $\times$ ) the upper end of the linear dynamic range, in particle size that produced signal intensities that were linearly proportional to the particle (analyte) mass, could be greatly extended. Not surprisingly, reducing the sensitivity increased the minimum size detectable particle. The results are consistent with SiO<sub>2</sub> particles as large as 5000 nm being completely vaporized in the ICP.

Received 27th November 2024  
Accepted 3rd February 2025

DOI: 10.1039/d4ja00425f

rs.c.li/jaas

## 1 Introduction

The use of single particle Inductively Coupled Plasma-Mass Spectrometry (spICP-MS) to determine particle number concentration, size (mass equivalent diameter) and elemental chemical composition continues to grow rapidly.<sup>1–5</sup> However, the vast majority of the applications reported to date using spICP-MS have focused on engineered nanoparticles, sometimes including their fate in the environment<sup>6–20</sup> and biological<sup>21–23</sup> systems.

When measuring engineered nanoparticles (diameters  $\leq$  100 nm): (1) the transport efficiency into the ICP does not depend on size; (2) typically the elemental composition of the particles is known and includes only one or two elements; (3) it is reasonable to assume that the nanoparticles are completely vaporized in the plasma under optimum conditions for analysis of solutions; and (4) the required linear dynamic range (for signal intensities), while wide, is typically within the range provided by most modern ICP-MS instruments capable of single particle detection (especially if analog rather than pulse counting measurements are used).

Measuring both polydisperse nanoparticles and microparticles with a wide range of unknown, highly variable elemental compositions is much more challenging. The transport efficiency from the sample to the nebulizer through the spray chamber and into the ICP may be dependent on the microparticle mass and/or size, complicating measurement of particle number concentrations as a function of size. For example, Ebdon *et al.*<sup>24–26</sup> showed that refractive particles larger than about 2000 nm may not be transported through a nebulizer/spray chamber into an ICP-OES. Using a high efficiency single cell spICP-MS introduction system<sup>27</sup> with an uptake rate of 10  $\mu$ L min<sup>–1</sup> resulted in 100%

<sup>a</sup>Trace Element Research Laboratory, School of Earth Sciences, The Ohio State University, Columbus, OH, 43210, USA. E-mail: olesik.2@osu.edu

<sup>b</sup>Department of Chemistry and Biochemistry, The Ohio State University, Columbus, OH, 43210, USA

<sup>c</sup>Byrd Polar and Climate Research Center, The Ohio State University, Columbus, OH, 43210, USA

<sup>d</sup>Department of Civil and Environmental Engineering, Carnegie Mellon University, Pittsburgh, PA, 15213, USA

<sup>e</sup>Center for Atmospheric Particle Studies, Carnegie Mellon University, Pittsburgh, PA, 15213, USA

<sup>f</sup>Honeybee Robotics, Blue Origin, Altadena, CA, 91001, USA

† Electronic supplementary information (ESI) available. See DOI: <https://doi.org/10.1039/d4ja00425f>



transport efficiency of cells up to  $\sim 3000$  nm and but lower transport efficiency for  $\sim 6400$  nm cells.<sup>28</sup> However, cells have a lower density than most particles.

If the microparticles are too large, they may not be completely vaporized, atomized, and ionized in the plasma which would lead to an underestimate of the total mass and size of the particle.<sup>29,30</sup> Olesik and Gray reported<sup>29</sup> that ICP-MS Si<sup>+</sup> signal intensity was linearly related to the mass of Si in SiO<sub>2</sub> particles with diameters only up to about 1  $\mu$ m, consistent with particles larger than 1  $\mu$ m not being completely vaporized in the plasma. However, Ebdon and Collier<sup>24</sup> provided evidence that refractory particles as large as 8  $\mu$ m were completely vaporized in ICP-OES when using a 3 mm inner diameter (i.d.) injector (center tube of the ICP torch).

Measurement of both nanoparticles (diameter  $\leq 100$  nm) and fine microparticles ( $100 \text{ nm} \leq d \leq 2500$  nm or more) requires a huge signal intensity dynamic range. The mass of a particle depends on the cube of its diameter. Therefore, the dynamic range (in mass or signal intensity) to measure particles with diameters from 10 nm to 2500 nm is at least  $1.6 \times 10^7$  (250<sup>3</sup>). To measure particles with diameters from 10 nm to 5000 nm the dynamic range needs to be at least  $1.3 \times 10^8$  (500<sup>3</sup>). In addition, because the sensitivity (counts per fg) is element dependent, an even larger linear dynamic range may be required. Furthermore, although some current ICP-Quadupole MS instruments are said to have a linear dynamic range up to  $\sim 10^{10}$  ( $\sim 10^{11}$  on some instruments) it is important to remember that is for a measurement time of at least one second.<sup>31</sup> For spICP-MS, typically dwell times of 2 ms or less are used, and the signal from ions produced from a single particle typically lasts for only  $\sim 0.3$  to 0.5 ms.<sup>5,29</sup>

The linear dynamic range provided by ICP-TOFMS instruments is typically<sup>32</sup>  $\sim 10^6$  (for a 1 second measurement time). Therefore, the dynamic range for 2 ms may be  $\sim 2000$  (and that assumes a constant intensity during the 2 ms). In reality, the signal from a vaporized, ionized particle typically has a roughly Gaussian shape (with a somewhat longer trailing tail due to diffusion of the ion cloud as it travels in the ICP to the sampling cone<sup>33–35</sup>) so the peak intensity will be larger than the average intensity.

Data illustrating the challenges due to particle size dependent transport efficiencies and a limited dynamic range, where signal intensity is linearly proportional to the particle analyte mass when measuring nanoparticles and microparticles, are discussed below. Sets of nearly monodisperse engineered particles (SiO<sub>2</sub> with diameters from 500 to 5000 nm and Au particles with diameters from 60 to 1500 nm) were used to explore particle transport efficiency from the nebulizer to the ICP and the linear dynamic range. Measurements at optimum and reduced sensitivity were used to distinguish nonlinearity due to incomplete particle vaporization from limited ion detection system linear dynamic range.

## 2 Experimental

### 2.1 Engineered nanoparticle and microparticle suspensions

Commercially available citrate-capped engineered Au and bare SiO<sub>2</sub> nanoparticle and microparticle suspensions were

purchased from BBI Solutions (Crumlin, United Kingdom), Nancomposix (California, USA), ThermoFisher Scientific (Waltham, Massachusetts, USA), or Bangs Laboratories (Indiana, USA) (details including densities of the engineered Au and SiO<sub>2</sub> (ref. 36 and 37) particles are in Table S1†). Suspensions were prepared by serial dilution (Table S1†) in deionized water (18.2 M $\Omega$  cm, produced by a ThermoFisher Scientific/Barnstead Smart2Pure Pro UV/UF 16 LPH system). Stock suspensions were placed in an ultrasonic bath for 10 minutes before dilution and then repeatedly inverted until settled particles were resuspended in an attempt ensure a homogeneous and agglomerate-free suspension. Each suspension was diluted  $12 \times$  to 7 640 000 $\times$  to contain a known number of particles ( $\sim 100$  000 to  $\sim 250$  000 particles per mL). The mean particle diameter and the mass concentration of Au or Si in the original stock suspension (provided by each manufacturer) or the particle number concentration (provided by the manufacturer) were used to calculate the number of particles per mL in the diluted particle suspensions. All particle suspensions were made gravimetrically using an electronic analytical balance (Mettler-Toledo XSR304, Greifensee, Switzerland).

### 2.2 Single particle inductively coupled plasma-mass spectrometers

Three commercially available spICP-MS instruments were used in this study: a PerkinElmer NexION 350D spICP-QMS (Thornhill, Ontario, Canada), a TOFWERK icpTOF-R spICP-TOFMS (Thun, Switzerland), and a Nu Instruments Vitesse spICP-TOFMS (Wrexham, United Kingdom). The NexION 350D and TOFWERK icpTOF-R used a 1.8 mm i.d. Meinhard (Golden, Colorado, USA) sapphire injector, an Elemental Scientific Inc. (Omaha, Nebraska, USA) 47 mm PFA barrel spray chamber with O-ring-free endcap, and an Elemental Scientific Inc. self-aspirating PFA-50 nebulizer without probe to deliver freely aspirated solutions and suspensions to the instrument with minimal joints in which particles may become stuck. An Elemental Scientific Inc. self-aspirating PFA-20 nebulizer without probe was also used for some measurements during spICP-QMS analysis. In one set of NexION 350D measurements, an Elemental Scientific Inc. PFA-ST nebulizer was used at an uptake rate of 340  $\mu$ L min<sup>-1</sup> with the suspension delivered to the nebulizer using a peristaltic pump. The Nu Instruments Vitesse used a cyclonic spray chamber and a glass, concentric nebulizer with sample pumped at 400  $\mu$ L min<sup>-1</sup>. Sample uptake rates on the NexION 350D and icpTOF-R were measured gravimetrically. Instrument parameters are listed in Table 1.

The nebulizer gas flow rate on each spICP-MS instrument was optimized to achieve maximum <sup>115</sup>In<sup>+</sup> sensitivity while maintaining a cerium oxide to cerium (<sup>140</sup>Ce<sup>16</sup>O<sup>+</sup>/<sup>140</sup>Ce<sup>+</sup>) ratio less than 3% using a multi-element solution standard containing 1  $\mu$ g L<sup>-1</sup> each of Be, Co, Ce, In, and U (on the NexION 350D) or 1  $\mu$ g L<sup>-1</sup> each of Co, In, Ce and U (on the TOFWERK icpTOF-R and Nu Instruments Vitesse). Decreasing the nebulizer gas flow rate and/or increasing the sampling depth would increase the time the sample spends in the hot plasma prior to the reaching the sampling orifice, potentially increasing the



Table 1 spICP-MS instrument parameters used in this study

	PerkinElmer NexION 350D		Nu instruments Vitesse		TOFWERK icpTOF-R	
Instrument type	spICP-QMS		spICP-TOFMS		spICP-TOFMS	
Plasma power (W)	1600		1300		1500	
Plasma gas (L min <sup>-1</sup> )	18		13		17	
Auxiliary gas (L min <sup>-1</sup> )	1.2		2.0		1.0	
Injector i.d. (mm)	1.8		1.8		1.8	
Nebulizer gas flow (L min <sup>-1</sup> )	1.09		1.00		1.00	
Sample uptake rate (μL min <sup>-1</sup> )	22, 60, or 340		~400		60	
Sampling depth (mm)	11		12		5	
Integration time, single particle (μs)	100		80		2000 <sup>a</sup>	
Sensitivity	Optimized <sup>c</sup>	Reduced <sup>c</sup>	Optimized <sup>d</sup>	Reduced <sup>d</sup>	Optimized <sup>e</sup>	Reduced <sup>e</sup>
Sensitivity reduction factor	1×	13×, 269×, or 182×	1×	30×	1×	11×
Mass resolution <sup>c</sup> ( $\Delta m$ , amu)	0.7	0.5, 0.2 or 0.15 <sup>b</sup>				
Beam attenuator <sup>d</sup>			1	30		
Extraction lens <sup>e</sup> 2 (V)					−290	−95

<sup>a</sup> Mass spectrum collected every 30 μs and then spectra summed over each 2000 μs. <sup>b</sup> Peak shape may be distorted at mass resolution of 0.2 or 0.15; as a result, the sensitivity reduction factor may be smaller for what is estimated to provide a smaller mass resolution. <sup>c</sup> PerkinElmer NexION 350D.

<sup>d</sup> Nu Instruments Vitesse. <sup>e</sup> TOFWERK icpTOF-R.

maximum particle size that could be completely vaporized in the plasma. However, the data discussed in this paper were always acquired at the optimum nebulizer gas flow rate for analysis of solutions (using the sampling depth listed in Table 1). No changes in the nebulizer gas flow rate or sampling depth were made to increase the time particles spent in the plasma.

The NexION 350D Quadrupole Ion Deflector (QID) was optimized for maximum sensitivity at low-, mid-, and high-masses. The Autolens function was then used for measurements. The icpTOF-R Extraction Lens 2 was optimized daily for maximum <sup>115</sup>In<sup>+</sup> sensitivity.

Si<sup>+</sup> intensity produced by SiO<sub>2</sub> particles was determined using *m/z* 28. The Au<sup>+</sup> intensity produced by Au particles was determined using *m/z* 197.

**2.2.1 Threshold used to identify signals produced by particles.** spICP-QMS or spICP-TOFMS can measure individual particles by differentiating the burst of signal produced by a particle (a “particle event”) from the quasi-continuous background. The signal from each particle must be greater than a threshold which uses the average quasi-continuous background signal ( $\mu$ ) which is determined using an iterative procedure to remove signals produced by particles<sup>38</sup> and the square root of the quasi-continuous background ( $I_b$ ) (eqn (1)).<sup>39–41</sup>

$$\text{Particle signal detection limit} = \mu + 3.29\sqrt{I_b} + 2.72 \quad (1)$$

While a mass dependent compound Poisson distribution may be more appropriate for spICP-TOFMS measurements,<sup>42</sup> the instrument software version we had did not include it.

**2.2.2 Mass/size dependent transport efficiency of nanoparticles and fine microparticles.** The transport efficiency is the fraction of particles in the sampled volume that are delivered to the nebulizer, pass through the spray chamber, and enter the plasma.<sup>38</sup> It is possible in some cases for particle losses to occur in the sample tubing or joints as the sample travels from the

sample to the nebulizer. The transport efficiency must be known or measured to calculate the particle number concentration (particles per volume of sample delivered to the ICP) and mass equivalent diameter of particles in each suspension (signal intensity in counts during calibration using solutions must be converted to sensitivity in counts per femtogram using the transport efficiency and volume of sample delivered to the nebulizer).

Transport efficiency is commonly determined using the Particle Frequency (Particle Number) method or the Particle Size (Solution/Nanoparticle) method, described in detail by Pace *et al.*<sup>38</sup> The Particle Number method is the ratio of the number of detected particles to the number delivered to the nebulizer (known # per mL in engineered particle suspension × uptake rate × measurement time). The Solution/Nanoparticle method estimates transport efficiency from the ratio of the solution sensitivity (in counts per fg delivered to the nebulizer) to the particle sensitivity (not affected by transport efficiency) in average counts per fg of analyte in the particle. The Solution/Nanoparticle method cannot be used to determine the size (or mass) dependent transport efficiency because it determines the transport efficiency of elements dissolved in the solution, not of the particles. Therefore, the Particle Frequency (Particle Number) method was used here.

**2.2.3 Optimized and reduced sensitivities.** The silicon (<sup>28</sup>Si<sup>+</sup>) sensitivity (in counts per femtogram (fg)) was determined for each instrument using engineered SiO<sub>2</sub> particles measured in analog mode under optimized conditions and then, using the same plasma conditions, with reduced sensitivity. Sensitivity was reduced by factors of 13×, 269×, or 182× on the NexION 350D spICP-QMS by changing the resolution ( $\Delta m$ ) from 0.7 amu to 0.5, 0.2, or 0.15 amu, respectively, for some measurements. Sensitivity was reduced by a factor of 11 during some measurements using the TOFWERK icpTOF-R spICP-TOFMS by changing the Extraction Lens 2 voltage from −290 V to −95 V.



Sensitivity was reduced by a factor of 30 using the beam attenuator during some measurements on the Nu Instruments Vitesse spICP-TOFMS<sup>43</sup> (Table 1).

## 3 Results and discussion

### 3.1 Mass/size-dependent transport efficiency of nanoparticles and microparticles

Engineered Au and SiO<sub>2</sub> particles with masses between 2 and 33 358 fg (diameters between 60 and 3170 nm) were measured by spICP-QMS using uptake rates of 27 and 60  $\mu\text{L min}^{-1}$ . Fig. 1 shows the particle transport efficiencies as a function of particle mass; the efficiencies are plotted as a function of particle diameter in Fig. S1.†

Au particles with diameters up to at least 200 nm and SiO<sub>2</sub> particles with diameters up to about 730 nm had similar transport efficiencies ( $\sim 30\%$ ) when an uptake rate of 27  $\mu\text{L min}^{-1}$  was used. The particle transport efficiency decreased dramatically for SiO<sub>2</sub> particles with diameters of 990 nm ( $\sim 1100$  fg) or more. The transport efficiency for SiO<sub>2</sub> particles with diameters larger than 2000 nm was more than five times smaller than for SiO<sub>2</sub> particles with diameters of 730 nm or smaller.

The particle transport efficiencies measured with an uptake rate of 60  $\mu\text{L min}^{-1}$  are consistently lower than at 27  $\mu\text{L min}^{-1}$ . This is likely because aerosol droplets can evaporate more extensively during their travel through the spray chamber when a lower uptake rate is used (resulting in smaller, more efficiently transported droplets) and the probability of droplet-droplet collisions/coagulation (resulting in larger, less efficiently transported droplets) is less likely at the lower uptake rate.<sup>44</sup> At an uptake rate of 60  $\mu\text{L min}^{-1}$ , the decrease in particle transport efficiency also appears to begin for particles with a smaller mass (diameter). For example, the transport efficiency of 690 nm SiO<sub>2</sub> particles was about half of the transport efficiency of 150 nm Au particle at an uptake rate of 60  $\mu\text{L min}^{-1}$  while the transport efficiency of 730 nm SiO<sub>2</sub> particles was similar to the transport efficiency of 200 nm Au particles or 480 nm SiO<sub>2</sub> when the

uptake rate was 27  $\mu\text{L min}^{-1}$ . The particle transport efficiencies will also be dependent on the sample introduction system used.

The implication of the behavior shown in Fig. 1 is that to measure both nanoparticles and microparticles in a sample, it is necessary to determine the particle size/mass-dependent transport efficiencies over the particle size/mass range of interest. A transport efficiency determined using nanoparticles (e.g. 60 nm Au) cannot be used to calculate the particle number concentration of particles larger than some uptake rate dependent mass or size. For example, using the 60 nm Au particle transport efficiency at sample uptake rates of 60 or 27  $\mu\text{L min}^{-1}$ , 22% and 31% respectively, to determine the number concentration of 3170 nm SiO<sub>2</sub> particles (transport efficiencies of  $\sim 4\%$ ) would result in an underestimation of the particle number concentration by more than 80%.

The particle transport efficiency is also dependent on the particle mass (or size) when a much higher sample uptake rate (340  $\mu\text{L min}^{-1}$ ) is used (Fig. S2†). As expected, the transport efficiency when the higher sample uptake rate is used is lower for all particle sizes than when lower sample uptake rates (such as 27 or 60  $\mu\text{L min}^{-1}$ ) are used.

### 3.2 Signal intensity versus particle (analyte) mass

There are at least two possible causes of a deviations from a linear relationship between signal intensity and particle analyte mass. Signal intensities would not be proportional to particle analyte mass if the particles are too large to be completely vaporized, atomized, and ionized in the plasma prior to reaching the sampling orifice.<sup>29,30,45–48</sup> Another possibility is that particles larger than some size (which may depend on the instrument, analyte element, and isotopic abundance) produce a signal outside of the instrument's ion detection system linear dynamic range (*i.e.* the analyte signal is not linearly related to the number of analyte ions produced in the plasma or the number of ions that reach the detector).

Typically, for nanoparticles (diameter  $\leq 100$  nm), the signal intensity is proportional to the mass of an analyte element, especially when using analog detection.<sup>49–51</sup> Non-linear behavior has been reported when measuring Au particles larger than 200 nm using an analog detector<sup>52,53</sup> and silica (SiO<sub>2</sub>) microparticles<sup>29,30,45–48</sup> larger than about 1  $\mu\text{m}$ .

**3.2.1 Pulse counting detection.** Pulse counting is often used to maximize the signal-to-noise ratio when measuring small signal intensities. However, the maximum intensity (in counts per s) that can be accurately measured in pulse counting mode by spICP-QMS (typically  $\sim 2$  million count per s,  $\sim 2000$  counts per ms,  $\sim 200$  counts per 0.1 ms) is limited by “pulse-pileup”.<sup>30,52</sup> When using pulse counting, the maximum accurately measurable Au nanoparticle can be as small as 40 nm.<sup>52</sup>

It is possible to somewhat extend the pulse-counting linear dynamic range by applying a “dead-time” correction.<sup>52</sup> In this case, the maximum accurately detectable Au particle size was increased from 40 nm to 60 nm.<sup>52</sup> An alternative way to extend the largest size (mass) particle that can be accurately measured is to use another ion that contains the analyte element but that produces a smaller signal (e.g. a minor isotope of the element or

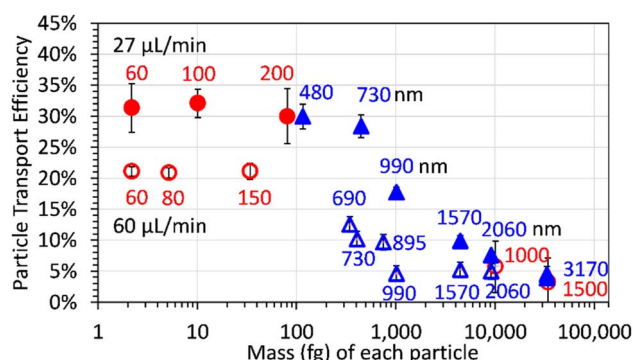


Fig. 1 Transport efficiency of engineered Au (●), and SiO<sub>2</sub> (▲) NPs and  $\mu\text{Ps}$  as a function of the mass (fg) of each particle measured by spICP-QMS at using an uptake rate of 27  $\mu\text{L min}^{-1}$  (filled symbols) and 60  $\mu\text{L min}^{-1}$  (open symbols). Nominal particle size (nm) is shown next to each point. Error bars indicate  $\pm$  one standard deviation of three measurements of transport efficiency.





a polyatomic ion containing the analyte element). For example, measuring  $\text{AuAr}^+$  instead of  $\text{Au}^+$  can also enable the measurement of larger Au particles (increasing from the maximum size within the linear dynamic range from 100 nm to 400 nm<sup>53</sup>) in pulse counting mode. The signal intensity of  $\text{AuAr}^+$  ions produced by particles was four orders of magnitude smaller than the intensity of  $\text{Au}^+$  elemental ions from the same size particle. These results show that Au particles as large as 400 nm in diameter are completely vaporized in the ICP so that the initially observed 40 nm limit was due a decrease in the ratio of analyte ions detected (counts) to analyte ions reaching the detector, not incomplete vaporization of 40 nm Au particles. However, when the sensitivity is reduced (by using  $\text{AuAr}^+$  or a minor isotope of an element that is not monoisotopic) means that smaller particles may not be detectable, thus increasing the low-end of the linear dynamic range.

**3.2.2 Analog detection on spICP-QMS.** Many current generation instruments (including the NexION 350D spICP-QMS), can measure particle signals using the analog mode of the detector to avoid problems due to “pulse-pileup” and thereby allow accurate measurement of signals that are too large to measure using pulse counting. spICP-TOFMS instruments detect an analog signal (current) which is converted to a digital number by an analog-to-digital converter. However, non-linear behavior was still observed for particles larger than ~895 nm (Fig. 2) when using analog mode detection.

Using optimized sensitivity (e.g., obtained by optimizing the nebulizer gas flow rate to produce the maximum  $^{115}\text{In}^+$  signal intensity from a solution standard containing In and Ce while keeping the  $\text{CeO}^+/\text{Ce}^+$  signal ratio below 3%), 500, 690, and 895 nm  $\text{SiO}_2$  particles produce a signal that increases proportionally (linearly) with the mass of Si in those particles, as shown in Fig. 2a, while the signal produced from 1050 nm  $\text{SiO}_2$  particles was slightly less than linearly proportional to the mass of Si. Signals produced from  $\text{SiO}_2$  particles with average diameters of 1050, 2060, and 3170 nm were about 15%, 35%, and 51%, respectively, smaller than expected from the linear regression line based on the signals produced by the 500, 690, and 895 nm  $\text{SiO}_2$  particles (Fig. 2b). The ratio of  $\text{Si}^+$  intensities produced by 2060 nm and 895 nm  $\text{SiO}_2$  particles (8100 counts/1100 counts = 7.36) is smaller than the ratio of Si mass in each particle standard (4270 fg/350 fg = 12.2).

Interestingly, Olesik and Gray also reported<sup>29</sup> a linear relationship between signal intensity and the particle mass for  $\text{SiO}_2$  particles smaller than 1  $\mu\text{m}$  using an analog current amplifier and a digital oscilloscope for analog to digital conversion and similar deviations from linearity for particles as large as ~2000 nm. They concluded that  $\text{SiO}_2$  particles larger than 1  $\mu\text{m}$  diameter may be incompletely vaporized in the plasma prior to reaching the sampling orifice. They did not consider the possibility of nonlinearity due to the ion detection system.

Because very short dwell times (0.1 ms) were used with the NexION 350D, the signal in units of counts per second is very large even when the total number of counts in the dwell times summed across the “particle event” may only be 2000 counts, as shown in the right y-axes of Fig. 2a and b. The approximate signals in units of counts per second were estimated by dividing the average  $\text{Si}^+$  intensity (summed across the peak in signal *versus* time for each detected particle) by the width of the particle event (~300  $\mu\text{s}$ ), not the maximum counts per second during the particle event signal. The  $\text{Si}^+$  signal produced from a 3170 nm  $\text{SiO}_2$  particle would be about 160 million counts per s if the signal was on the same linear regression line as the 500, 690, and 895 nm  $\text{SiO}_2$  particles.

Subsequently, we made another set of measurements with  $\text{SiO}_2$  particles from 690 to 5000 nm (Fig. S3†). The results are consistent with those shown in Fig. 2; particles with diameters of 1050 nm or more produce signals that are less than proportional to the mass of Si in the particle. The deviation from linearity increases for 2060 nm, 3170 nm, and 5010 nm  $\text{SiO}_2$  particles.

**3.2.3 spICP-TOFMS.** Both the TOFWERK icpTOF-R spICP-TOFMS (Fig. 3a and b) and Nu Instrument Vitesse spICP-TOFMS (Fig. 3c and d) also exhibited deviations from a linear relationship between  $\text{Si}^+$  analog signal intensity and Si mass for  $\text{SiO}_2$  particles larger than ~730 nm using the icpTOF-R (Fig. 3a) and ~895 nm using the Vitesse (Fig. 3c) measured using optimized conditions. Signal intensities began to deviate from linearity on all three instruments when the sum of counts due to a particle were higher than around 1000 counts: starting somewhere between about 1100 and 1400 counts on the NexION 350D (Fig. 2a), between about 1000 and 1400 counts on the TOFWERK icpTOF-R (Fig. 3a), and between about 700 and 800 counts on the Vitesse (Fig. 3c).

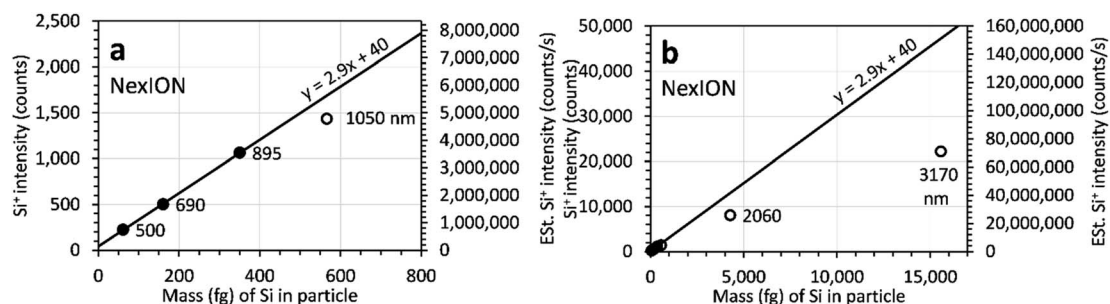
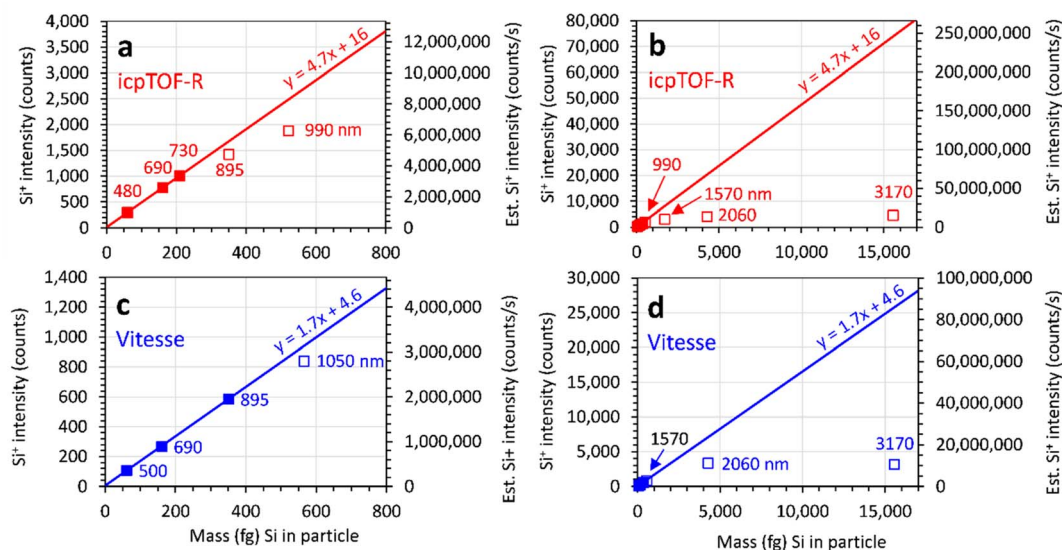


Fig. 2  $^{28}\text{Si}^+$  signal in counts (left y-axis) and estimated counts per s (right y-axis) as a function of Si mass in particle produced by engineered  $\text{SiO}_2$  particles measured by spICP-QMS using optimized sensitivity for particles with: (a) masses less than 800 fg and (b) masses less than 17 000 fg. The nominal particle diameter is shown next to each point. Filled symbols indicate particles used to calculate the linear regression line while open symbols indicate particles not used to calculate the linear regression line.





**Fig. 3**  $^{28}\text{Si}^+$  signal in counts (left y-axis) and estimated counts per s (right y-axis) produced by engineered  $\text{SiO}_2$  particle suspensions measured by: (a and b) TOFWERK icpTOF-R and (c and d) Nu Instruments Vitesse spICP-TOFMS using optimized sensitivity for particles with: (a and c) masses less than 800 fg and (b and d) masses less than 17 000 fg. The nominal particle diameter is shown next to each point. Filled symbols indicate particles used to calculate the linear regression line while open symbols indicate particles not used to calculate the linear regression line.

When particles produce signal outside of the linear dynamic range of the instrument, it is impossible to accurately determine the particle mass equivalent diameter using a linear calibration. For example, the mass equivalent diameter of 3170 nm  $\text{SiO}_2$  particles would be underestimated by 25%, 61%, and 51%, respectively, on the NexION (Fig. 2b), icpTOF-R (Fig. 3b), and Vitesse (Fig. 3d) when the optimized sensitivity is used. Furthermore, different sized particles that produce signals outside of the instrument linear dynamic range may produce similar signals. For example, the average  $\text{Si}^+$  signal produced by 3170 nm  $\text{SiO}_2$  particles ( $\sim 3200$  counts) using the Vitesse was smaller than the average  $\text{Si}^+$  signal produced by smaller (2060 nm)  $\text{SiO}_2$  particles ( $\sim 3300$  counts) (Fig. 3d).

**3.2.4 Reduced spICP-QMS sensitivity.** Deviations from linearity of particle signal intensity *versus* the mass of the analyte element in each particle are often attributed to incomplete particle vaporization.<sup>29,30</sup> However, as was the case discussed above when pulse counting was used to measure Au particles larger than 40 nm, another possibility is that the deviations are due to a decrease in the average measured signal per ion reaching the detector. To assess if the deviations from linearity seen in Fig. 2 and 3 could be due to the ion detection system, rather than incomplete particle vaporization, measurements were made with reduced sensitivities.

By reducing the NexION 350D  $\text{Si}^+$  sensitivity by  $269\times$  (using  $\Delta m = 0.2$  amu instead of  $0.7$  amu) the 2060 nm and 3170 nm  $\text{SiO}_2$  particles produce  $\text{Si}^+$  signals (47 counts and 169 counts, respectively) that are linear and proportional to the average mass of Si (4272 fg and 15 567 fg of Si, respectively) in those particles (Fig. 4). The ratio of the average  $\text{Si}^+$  signal produced by 3170 nm particles to the average  $\text{Si}^+$  signal produced by 2060 nm  $\text{SiO}_2$  particles ( $169 \text{ counts}/47 \text{ counts} = 3.60$ ) is almost the same as the ratio of the Si masses in 3170 nm and 2060 nm  $\text{SiO}_2$

particles ( $15\,567 \text{ fg}/4272 \text{ fg} = 3.62$ ). This is consistent with complete vaporization of the particles.

Reducing the sensitivity to measure larger particles within the linear dynamic range of the ion detection system increases the minimum size particle that can be accurately measured. As a result, the average  $\text{Si}^+$  intensities produced by the 895 and 1050 nm  $\text{SiO}_2$  particles (Fig. 4) were larger than expected (based on the linear regression line fit to the 2060 and 3170 nm particles). The average  $\text{Si}^+$  signals of 895 nm ( $\sim 18.7$  counts) and 1050 nm ( $\sim 19.4$  counts)  $\text{SiO}_2$  particles are above the linear regression line using  $269\times$  reduced sensitivity because many of the particles in the suspensions produce signals that are below the detection limit. The manufacturer specifies<sup>54</sup> the relative standard deviation (RSD) of the particle diameters to be 10%

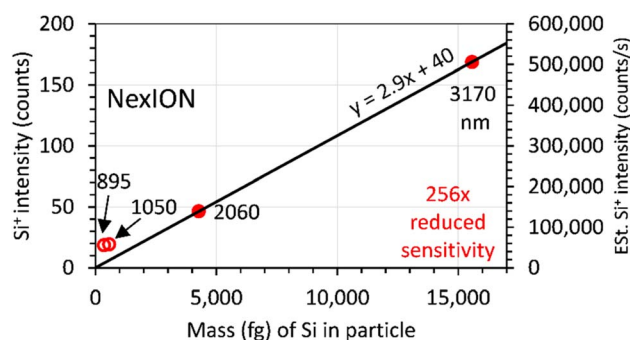


**Fig. 4**  $^{28}\text{Si}^+$  signal in counts (left y-axis) and estimated counts per s (right y-axis) produced by engineered  $\text{SiO}_2$  particle suspensions measured by a PerkinElmer NexION 350D spICP-QMS with highly reduced sensitivity ( $269\times$  compared to optimized sensitivity). Nominal particle diameter is shown next to each point. Filled symbols indicate particles used to calculate the linear regression line while open symbols indicate particles not used to calculate the linear regression line.



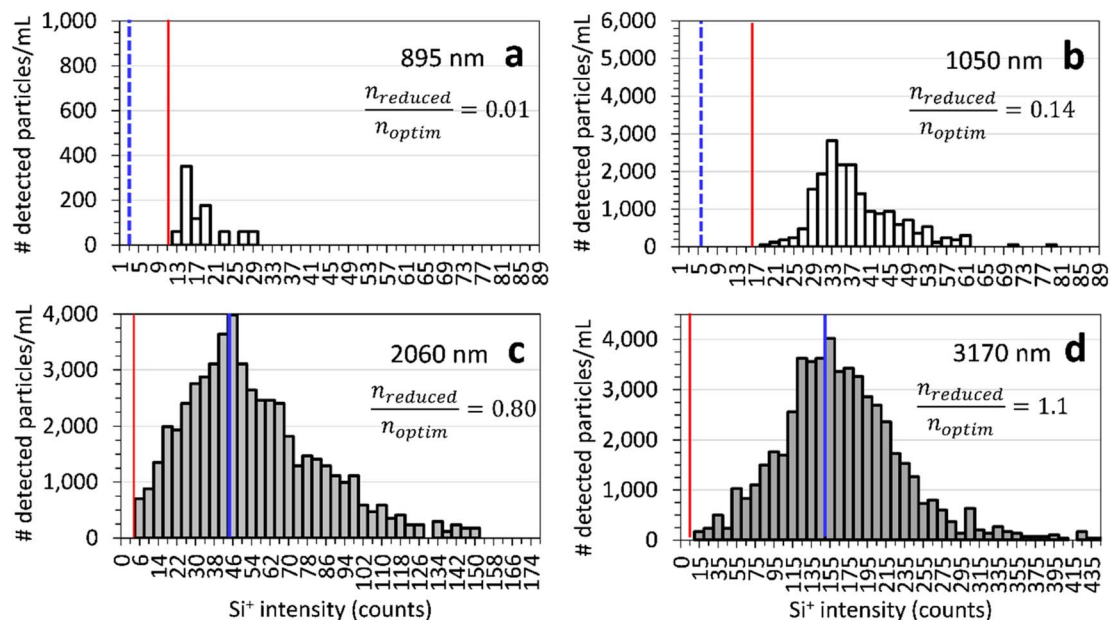


Fig. 5 Particle number concentration (particles per mL) versus  $\text{Si}^+$  intensity of (a) 895 nm, (b) 1050 nm, (c) 2060 nm, and (d) 3170 nm  $\text{SiO}_2$  particles measured by spICP-QMS with reduced sensitivity (269 $\times$  compared to optimized sensitivity). The expected average  $\text{Si}^+$  intensity produced by 895 nm and 1050 nm particles (---) (based on their size and the sensitivity calculated from the 3170 nm average intensity) is shown on plots (a and b). The measured average  $\text{Si}^+$  intensity (—) is shown on plots (c and d). The signal threshold to detect a particle event (—) is shown on each plot.  $n_{\text{reduced}}$  is the number of particles detected using 256 $\times$  reduced sensitivity.  $n_{\text{optim}}$  is the number of particles detected using the optimized sensitivity.

(corresponding to a 33% RSD in the particle masses). Fig. 5 shows the detected distribution of  $\text{Si}^+$  intensities produced from the particles with four different average diameters. As shown in Fig. 5a, the expected average  $\text{Si}^+$  signal intensity produced by 895 nm  $\text{SiO}_2$  (based on the counts per fg calculated from the sensitivity (counts per s) determined from the 3170 nm average intensity) is below the detection limit. As a result, only particles on the very upper end of the particle size distribution were detected, resulting in a higher than expected average signal.<sup>14,55</sup> Only 1% as many 895 nm  $\text{SiO}_2$  particles were detected when the sensitivity was reduced 269 $\times$  as when the optimum sensitivity was used. Only 14% as many 1050 nm particles were measured when the sensitivity was reduced 269 $\times$  as when the optimized sensitivity was used. For the 2060 nm particles, less than 20% of the particles on the lower end of the particle size were below the detection limit, having little effect on the average signal intensity.

$\text{SiO}_2$  particles with an average diameter greater than about 895 nm were beyond the linear dynamic range when the optimum sensitivity was used (Fig. 2) while  $\text{SiO}_2$  particles smaller than around 2000 nm were too small to be accurately measured when the sensitivity was reduced by 269 $\times$ . Therefore, an intermediate sensitivity is needed to accurately measure these particles. Fig. S3† shows the measured  $\text{Si}^+$  signal intensities as a function of the mass of Si in the particles when the sensitivity is reduced by 13 $\times$ .  $\text{SiO}_2$  particles with diameters from 690 to 990 nm are linearly related to the Si mass in the particle. Average  $\text{Si}^+$  signals produced by  $\text{SiO}_2$  particles larger than 990 nm are smaller than expected for a linear, proportional relationship between signal and mass of Si in the particle.

Therefore, the sensitivity must be reduced by more than 13 $\times$  to extend the linear dynamic range to particles up to 2000 nm.

It is possible to extend the linear dynamic range of the instrument by combining measurements made with different sensitivities. The sensitivity reduction factors (determined from the ratio of the slopes of each linear regression line) can be used to transform the signals made at reduced sensitivity to the same scale as the optimized sensitivity so that all the measured intensities can be plotted on a single line (Fig. 6). This approach is analogous to the dual detector calibration used to produce a single calibration line from signals measured following the final dynode (resulting in the highest gain) by pulse counting and by analog measurement of the detector current about midway through the set of dynodes (resulting in a lower gain).

The data in Fig. 4 and 6 are consistent with  $\text{SiO}_2$  particles with diameters of 3170 nm or less being completely vaporized in the ICP. In a subsequent set of measurements, we investigated  $\text{SiO}_2$  particles as large as 5010 nm in diameter (Fig. S3† shows data with optimized sensitivity,  $\Delta m = 0.7$  amu). When the sensitivity was reduced, the largest  $\text{SiO}_2$  particle that still produced a signal that was linearly proportional to the mass of Si in the particle increased. Reducing the sensitivity by 13 $\times$  (using  $\Delta m = 0.5$ ),  $\text{SiO}_2$  particles as large as 990 nm produced signals that were linearly proportional to the mass of Si in the particle (Fig. S4†). Larger particles (diameters  $\geq 1570$  nm) produced smaller signals than expected.

Reducing the sensitivity by 182 $\times$  (using  $\Delta m = 0.15$ ), provides results that are consistent with  $\text{SiO}_2$  particles nearly as large as 5010 nm being completely vaporized in the ICP (Fig. 7).





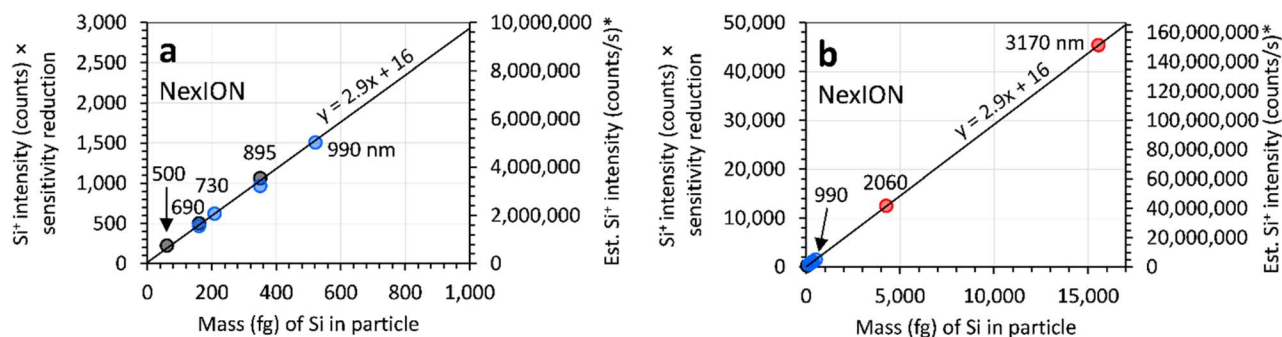


Fig. 6  $^{28}\text{Si}^+$  signal multiplied by the sensitivity reduction factor in counts (left y-axis) and estimated counts per s if no sensitivity reduction (counts per s multiplied by the sensitivity reduction factor) (right y-axis) produced by engineered  $\text{SiO}_2$  particle suspensions measured by a PerkinElmer NexION 350D spICP-QMS with optimized sensitivity (●),  $13\times$  reduced sensitivity (●) and  $269\times$  reduced sensitivity (●) for: (a) particles with masses less than 1000 fg, and (b) particles with Si masses less than 17,000 fg. A linear regression line (—) was calculated using the  $\text{Si}^+$  intensity  $\times$  sensitivity reduction factor and mass of all plotted particles.

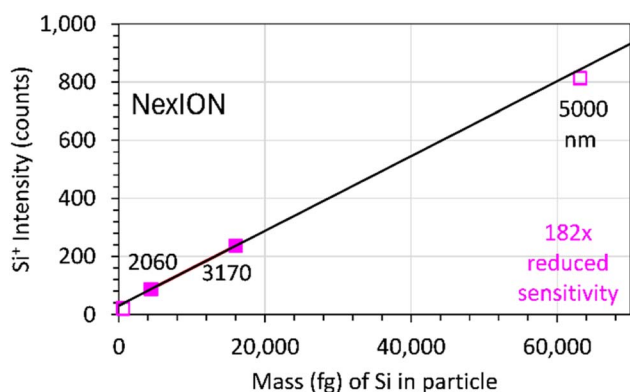


Fig. 7  $^{28}\text{Si}^+$  signal in counts produced by engineered  $\text{SiO}_2$  particles measured by spICP-QMS using  $182\times$  reduced sensitivity. The nominal particle diameter is shown next to each point. Filled symbols indicate particles used to calculate the linear regression line while open symbols indicate particles not used to calculate the linear regression line.

However,  $\text{SiO}_2$  particles with diameters  $\leq 1050$  nm produced signals that were too small to accurately measure.

**3.2.5 Reduced spICP-TOFMS sensitivity.**  $\text{SiO}_2$  particles were also measured with reduced sensitivity using the icpTOF-R and the Vitesse (Fig. 8). Using optimized conditions on the icpTOF-R, only 690 nm, and 730 nm  $\text{SiO}_2$  particles produced  $\text{Si}^+$  signals linearly proportional to the mass of Si in each particle (Fig. 3a). Using  $11\times$  reduced sensitivity, the 690 nm, 730 nm, 895 nm, 990 nm, and 1570 nm  $\text{SiO}_2$  particles produced  $\text{Si}^+$  signals that were linearly proportional to the mass of Si in each particle (Fig. 6a and b). The average  $\text{Si}^+$  intensity of 480 nm  $\text{SiO}_2$  particles is higher than expected for the same reasons as discussed above (see Fig. 5).

The Nu Instruments Vitesse spICP-TOFMS has an ion beam attenuator<sup>56</sup> that uses grids to attenuate the ion beam current by  $\sim 30\times$  or  $\sim 1000\times$ , independent of  $m/z$ . Using optimized conditions (no attenuation), only the 500 nm, 690 nm, and 895 nm  $\text{SiO}_2$  particles produced  $\text{Si}^+$  signals that were linearly proportional to the mass of each particle (Fig. 3c and d). Using reduced sensitivity, the 895 nm, 1050 nm, and 2060 nm  $\text{SiO}_2$  particles

produced average  $\text{Si}^+$  signals within the linear dynamic range of the instrument (Fig. 8c and d). The average  $\text{Si}^+$  intensities of the 500 nm and 690 nm  $\text{SiO}_2$  particles were overestimated due to the threshold cutting off lower intensity particle signals from the average intensity (similar to the data shown in Fig. 4). Using the ratio of particle number concentration measured using reduced sensitivity to optimized sensitivity,  $\sim 96\%$  and  $66\%$  of 500 nm and 690 nm  $\text{SiO}_2$  particles, respectively, were below the threshold. Further reducing sensitivity of both the icpTOF-R and Vitesse could ensure that all large  $\text{SiO}_2$  particles that are completely vaporized produce  $\text{Si}^+$  signal within the linear dynamic range. However, using reduced sensitivity, smaller  $\text{SiO}_2$  particles may not produce enough signal above the threshold to be accurately measured. It may be necessary to measure particle suspensions using both optimized sensitivity (for smaller particles) and one or more reduced sensitivities.

Au particles with diameters from 60 nm to 1500 nm were also measured with optimized sensitivity (Fig. S5a and b†) and  $22\times$  reduced sensitivity (Fig. S5c and d†) using the TOFWERK icpTOF-R. With optimized sensitivity only particles up to 150 nm in diameter produced signals that were linearly proportional to the Au mass in the particles (Fig. S5a and b†). The signals for Au particles with diameters from 150 nm to 1000 nm increase nonlinearly. Even though the ion detection system could measure more than 14 000 counts, the relationship between Au mass and signal intensity became nonlinear at around 1400 counts. Perhaps a non-linear calibration function could be used to measure particles that produced signals greater than  $\sim 1400$  counts but less than  $\sim 10\,000$  counts; this requires further investigation. The average signal intensity from 1000 nm Au particles was larger than the signal produced from 1500 nm Au particles. The largest Au particle within the linear range was 300 nm when the sensitivity was reduced by  $22\times$ . The signals produced from 400 to 1500 nm Au particles were smaller than expected (Fig. S2b and S3d†) but closer to the expected signals than when optimized sensitivity was used. Further reduction in sensitivity, or perhaps a nonlinear calibration, would be needed to obtain the correct Au particle diameter based on the measured signal intensities.





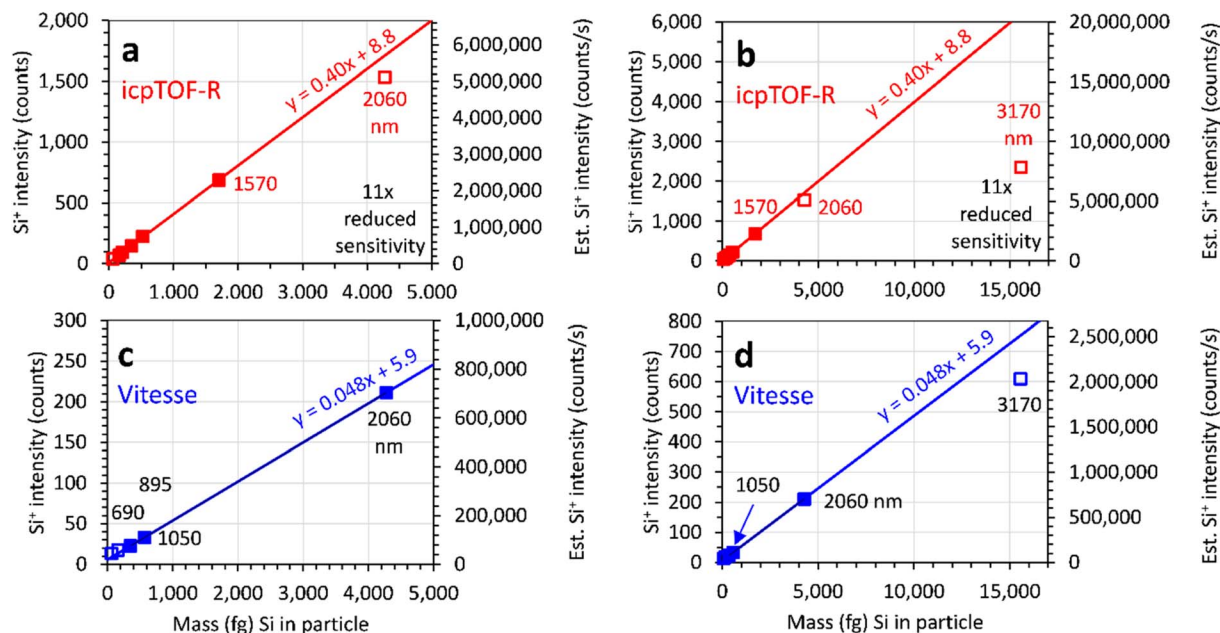


**Fig. 8**  $^{28}\text{Si}^+$  signal in counts (left y-axis) and estimated counts per s (right y-axis) produced by  $\text{SiO}_2$  particle suspensions measured using: (a and b) TOFWERK icpTOF-R and (c and d) Nu Instruments Vitesse spICP-TOFMS using reduced sensitivity for particles with diameters: (a and c) up to 2060 nm and (b and d) up to 3170 nm. icpTOF-R sensitivity was reduced 11 $\times$  and Vitesse sensitivity was reduced 30 $\times$  from the optimized sensitivity on each instrument. Nominal particle diameter is shown next to each point. Filled symbols indicate particles used to calculate the linear regression line while open symbols indicate particles not used to calculate the linear regression line.

## 4 Conclusions

The particle transport efficiency may be dependent on the particle size when a nebulizer/spray chamber sample introduction system is used. For the sample introduction system used in this study, the transport efficiency for  $\text{SiO}_2$  particles larger than 700 to 800 nm fell off dramatically as the particle diameter increased. The transport efficiency cannot be measured using nanoparticles (such as 60 nm Au) to accurately estimate the transport efficiency of particles larger than 700 to 800 nm. Therefore, the transport efficiency of larger particles must be experimentally determined as a function of particle size (mass). Furthermore, the Particle Frequency (Particle Number) based method must be used. The Particle Size (Solution/Nanoparticle) method measures the particle transport efficiency of elements dissolved in the solution and therefore cannot be used to determine the particle transport efficiency as a function of particle size (mass). The particle transport efficiency is also strongly dependent on the sample uptake rate when a nebulizer/spray chamber sample introduction system is used.<sup>44</sup>

We have presented evidence that  $\text{SiO}_2$  particles as large as 5000 nm in diameter are completely vaporized in the ICP. The linear dynamic range for particle measurement using spICP-QMS or spICP-TOFMS is limited more by the ion detection system than by incomplete particle vaporization for  $\text{SiO}_2$  particles. Reducing instrument sensitivity (while keeping plasma conditions the same) can extend the upper end of the linear dynamic range enough to accurately measure engineered  $\text{SiO}_2$

particles at least large as 5000 nm (the largest size tested in this study).

The development of commercial spICP-TOFMS instruments is an important step forward in single particle analysis. This technique has the potential to, with important considerations and limitations, quickly measure the elemental compositions, mass equivalent size distributions, and number concentrations of thousands of individual nanoparticles and microparticles in minutes using small (less than 10 mL) sample volumes in a variety of environmental and industrial suspensions containing polydisperse, multi-element nanoparticles and microparticles. However, the particle size (mass) dependent particle transport efficiency of microparticles and the limited linear dynamic range of spICP-QMS and spICP-TOFMS must be accounted for to obtain accurate microparticle number concentrations, sizes, and elemental compositions.

Other considerations, including element and sample dependent detection limits and the effect of sample dependent background signal intensities (the quasi-continuous background that particle signals need to be distinguished from) must also be considered to accurately measure and compare measured particle number concentrations, the elemental compositions of particles, and the particle mass equivalent diameters. Some of these considerations will be the subject of a future publication.

## Data availability

The data supporting this article have been included as part of the ESI.<sup>†</sup>



## Author contributions

JWO and MLV conceived and planned this research. MLV and LMC made most of the measurements. PG was the original PI on the NSF grant that partially funded this research. SK provided Coulter counter measurements to confirm the particle number concentrations in some of the engineered particle suspensions. The first draft of this manuscript was taken in part from MLV's thesis. JWO wrote the final manuscript with editing input from MLV, LMC, and PG. JW was involved in key discussions about the results from the TOFWERK spICP-TOFMS and provided help in troubleshooting the instrument. RS and GVL allowed us to use the TOFWERK spICP-TOFMS in their laboratory. All authors provided input on the manuscript.

## Conflicts of interest

The authors declare that they have no known competing financial interests or personal relationships that could have appeared to influence the work reported in this paper.

## Acknowledgements

Funding support for JWO, MLV, LMC, and SK was provided in part by NSF Award 1744961. PerkinElmer is thanked for providing the NexION 350 ICP-MS and for partial funding support for JWO, MLV, and LMC. The Carnegie Mellon University Center for Atmospheric Particle Studies and Department of Civil and Environmental Engineering is thanked for use of the TOFWERK spICP-TOFMS instrument. Lukas Schlatt of Nu Ametek is thanked for making the measurements on the Vitesse spICP-TOFMS and sharing the data with us. JW acknowledges the Swiss National Science Foundation for funding this research under the Postdoctoral Mobility program (Project No. P500PN\_202844).

## References

- 1 F. Laborda, E. Bolea and J. Jiménez-Lamana, Single Particle Inductively Coupled Plasma Mass Spectrometry: A Powerful Tool for Nanoanalysis, *Anal. Chem.*, 2014, **86**, 2270–2278.
- 2 D. Mozhayeva and C. Engelhard, A critical review of single particle inductively coupled plasma mass spectrometry – A step towards an ideal method for nanomaterial characterization, *J. Anal. At. Spectrom.*, 2020, **35**, 1740–1783.
- 3 X. Tian, H. Jiang, L. Hu, M. Wang, W. Cui, J. Shi, G. Liu, Y. Yin, Y. Cai and G. Jiang, Simultaneous multi-element and multi-isotope detection in single-particle ICP-MS analysis: Principles and applications, *Trends Anal. Chem.*, 2022, **157**, 116746.
- 4 J. Olesik, Single Particle ICP-MS: From Engineered Nanoparticles to Natural Nanoparticles, *Spectroscopy*, 2020, **35**, 20–22.
- 5 M. D. Montañó, J. W. Olesik, A. G. Barber, K. Challis and J. F. Ranville, Single Particle ICP-MS: Advances toward routine analysis of nanomaterials, *Anal. Bioanal. Chem.*, 2016, **408**, 5053–5074.
- 6 J. Vidmar, T. Zuliani, R. Milačič and J. Ščančar, Following the Occurrence and Origin of Titanium Dioxide Nanoparticles in the Sava River by Single Particle ICP-MS, *Water*, 2022, **14**, 959.
- 7 L. Hendriks and D. M. Mitrano, Direct Measurement of Microplastics by Carbon Detection *via* Single Particle ICP-TOFMS in Complex Aqueous Suspensions, *Environ. Sci. Technol.*, 2023, **57**, 7263–7272.
- 8 M. D. Montañó, C. W. Cuss, H. M. Holliday, M. B. Javed, W. Shoty, K. L. Sobocinski, T. Hofmann, F. v. d. Kammer and J. F. Ranville, Exploring Nanogeochemical Environments: New Insights from Single Particle ICP-TOFMS and AF4-ICPMS, *ACS Earth Space Chem.*, 2022, **6**, 943–952.
- 9 H. Karkee and A. Gundlach-Graham, Characterization and Quantification of Natural and Anthropogenic Titanium-Containing Particles Using Single-Particle ICP-TOFMS, *Environ. Sci. Technol.*, 2023, **57**, 14058–14070.
- 10 L. N. Rand, *Using Single Particle ICP-MS to Study Occurrence and Behavior of Engineered, Natural, and Incidental Nanoparticles in Freshwater Streams*, Colorado School of Mines, Arthur Lakes Library, 2019.
- 11 J. Xu, C. Chen, X. Hu, D. Chen, G. Bland, J. Wielinski, R. Kaegi, D. Lin and G. V. Lowry, Particle-Scale Understanding of Arsenic Interactions with Sulfidized Nanoscale Zerovalent Iron and Their Impacts on Dehalogenation Reactivity, *Environ. Sci. Technol.*, 2023, **57**, 21917–21926.
- 12 S. Bevers, M. D. Montañó, L. Rybicki, T. Hofmann, F. von der Kammer and J. F. Ranville, Quantification and Characterization of Nanoparticulate Zinc in an Urban Watershed, *Front. Environ. Sci.*, 2020, **8**, DOI: [10.3389/fenvs.2020.00084](https://doi.org/10.3389/fenvs.2020.00084).
- 13 Y. Huang, A. A. Keller, P. Cervantes-Avilés and J. Nelson, Fast Multielement Quantification of Nanoparticles in Wastewater and Sludge Using Single-Particle ICP-MS, *ACS ES&T Water*, 2021, **1**, 205–213.
- 14 A. J. Goodman, A. Gundlach-Graham, S. G. Bevers and J. F. Ranville, Characterization of nano-scale mineral dust aerosols in snow by single particle inductively coupled plasma mass spectrometry, *Environ. Sci.: Nano*, 2022, **9**, 2638–2652.
- 15 G. D. Bland, P. Zhang, E. Valsami-Jones and G. V. Lowry, Application of Isotopically Labeled Engineered Nanomaterials for Detection and Quantification in Soils *via* Single-Particle Inductively Coupled Plasma Time-of-Flight Mass Spectrometry, *Environ. Sci. Technol.*, 2022, **56**, 15584–15593.
- 16 G. D. Bland, M. Battifarano, A. E. Pradas del Real, G. Sarret and G. V. Lowry, Distinguishing Engineered TiO<sub>2</sub> Nanomaterials from Natural Ti Nanomaterials in Soil Using spICP-TOFMS and Machine Learning, *Environ. Sci. Technol.*, 2022, **56**, 2990–3001.
- 17 G. D. Bland and G. V. Lowry, Multistep Method to Extract Moderately Soluble Copper Oxide Nanoparticles from Soil for Quantification and Characterization, *Anal. Chem.*, 2020, **92**, 9620–9628.



- 18 J. Xu, G. D. Bland, Y. Gu, H. Ziaei, X. Xiao, A. Deonarine, D. Reible, P. Bireta, T. P. Hoelen and G. V. Lowry, Impacts of Sediment Particle Grain Size and Mercury Speciation on Mercury Bioavailability Potential, *Environ. Sci. Technol.*, 2021, **55**, 12393–12402.
- 19 T. Erhardt, C. M. Jensen, O. Borovinskaya and H. Fischer, Single Particle Characterization and Total Elemental Concentration Measurements in Polar Ice Using Continuous Flow Analysis-Inductively Coupled Plasma Time-of-Flight Mass Spectrometry, *Environ. Sci. Technol.*, 2019, **53**, 13275–13283.
- 20 S. E. Szakas, K. Menking-Hoggatt, T. Trejos and A. Gundlach-Graham, Elemental Characterization of Leaded and Lead-Free Inorganic Primer Gunshot Residue Standards Using Single Particle Inductively Coupled Plasma Time-of-Flight Mass Spectrometry, *Appl. Spectrosc.*, 2023, **77**, 873–884.
- 21 L. Hendriks, V. M. Kissling, T. Buerki-Thurnherr and D. M. Mitrano, Development of single-cell ICP-TOFMS to measure nanoplastics association with human cells, *Environ. Sci.: Nano*, 2023, **10**, 3439–3449.
- 22 S. Rodrigues, A. Avellan, G. D. Bland, M. C. R. Miranda, C. Larue, M. Wagner, D. A. Moreno-Bayona, H. Castillo-Michel, G. V. Lowry and S. M. Rodrigues, Effect of a Zinc Phosphate Shell on the Uptake and Translocation of Foliarly Applied ZnO Nanoparticles in Pepper Plants (*Capsicum annuum*), *Environ. Sci. Technol.*, 2024, **58**, 3213–3223.
- 23 M. Baccaro, M. D. Montaña, X. Cui, A. Mackevica, I. Lynch, F. von der Kammer, R. W. Lodge, A. N. Khlobystov and N. W. van den Brink, Influence of dissolution on the uptake of bimetallic nanoparticles Au@Ag-NPs in soil organism *Eisenia fetida*, *Chemosphere*, 2022, **302**, 134909.
- 24 L. Ebdon and A. R. Collier, Particle size effects on kaolin slurry analysis by inductively coupled plasma-atomic emission spectrometry, *Spectrochim. Acta, Part B*, 1988, **43**, 355–369.
- 25 L. Ebdon, M. E. Foulkes and S. Hill, Direct atomic spectrometric analysis by slurry atomisation. Part 9. Fundamental studies of refractory samples, *J. Anal. At. Spectrom.*, 1990, **5**, 67–73.
- 26 P. Goodall, M. E. Foulkes and L. Ebdon, Slurry nebulization inductively coupled plasma spectrometry-the fundamental parameters discussed, *Spectrochim. Acta, Part B*, 1993, **48**, 1563–1577.
- 27 A. S. Groombridge, S.-i. Miyashita, S.-i. Fujii, K. Nagasawa, T. Okahashi, M. Ohata, T. Umemura, A. Takatsu, K. Inagaki and K. Chiba, High Sensitive Elemental Analysis of Single Yeast Cells (*Saccharomyces cerevisiae*) by Time-Resolved Inductively-Coupled Plasma Mass Spectrometry Using a High Efficiency Cell Introduction System, *Anal. Sci.*, 2013, **29**, 597–603.
- 28 S.-i. Miyashita, A. S. Groombridge, S.-i. Fujii, A. Minoda, A. Takatsu, A. Hioki, K. Chiba and K. Inagaki, Highly efficient single-cell analysis of microbial cells by time-resolved inductively coupled plasma mass spectrometry, *J. Anal. At. Spectrom.*, 2014, **29**, 1598–1606.
- 29 J. W. Olesik and P. J. Gray, Considerations for measurement of individual nanoparticles or microparticles by ICP-MS: determination of the number of particles and the analyte mass in each particle, *J. Anal. At. Spectrom.*, 2012, **27**, 1143.
- 30 W.-W. Lee and W.-T. Chan, Calibration of single-particle inductively coupled plasma-mass spectrometry (SP-ICP-MS), *J. Anal. At. Spectrom.*, 2015, **30**, 1245–1254.
- 31 PerkinElmer, NexION 5000 Multi-Quadrupole ICP Mass Spectrometer, <https://www.perkinelmer.com/product/final-assy-nexion-5000-n8160010>.
- 32 L. Hendriks, A. Gundlach-Graham, B. Hattendorf and D. Günther, Characterization of a new ICP-TOFMS instrument with continuous and discrete introduction of solutions, *J. Anal. At. Spectrom.*, 2017, **32**, 548–561.
- 33 M. P. Dziewatowski, L. B. Daniels and J. W. Olesik, Time-Resolved Inductively Coupled Plasma Mass Spectrometry Measurements with Individual, Monodisperse Drop Sample Introduction, *Anal. Chem.*, 1996, **68**, 1101–1109.
- 34 J. W. Olesik, Investigating the Fate of Individual Sample Droplets in Inductively Coupled Plasmas, *Appl. Spectrosc.*, 1997, **51**, 158A–175A.
- 35 I. I. Stewart, C. E. Hensman and J. W. Olesik, Influence of Gas Sampling on Analyte Transport within the ICP and Ion Sampling for ICP-MS Studied Using Individual, Isolated Sample Droplets, *Appl. Spectrosc.*, 2000, **54**, 164–174.
- 36 V. Masalov, N. Sukhinina, E. Kudrenko and G. Emelchenko, Mechanism of formation and nanostructure of Stöber silica particles, *Nanotechnology*, 2011, **22**, 275718.
- 37 K. Nozawa, H. Gailhanou, L. Raison, P. Panizza, H. Ushiki, E. Sellier, J. P. Delville and M. H. Delville, Smart Control of Monodisperse Stöber Silica Particles: Effect of Reactant Addition Rate on Growth Process, *Langmuir*, 2005, **21**, 1516–1523.
- 38 H. E. Pace, N. J. Rogers, C. Jarolimek, V. A. Coleman, C. P. Higgins and J. F. Ranville, Determining Transport Efficiency for the Purpose of Counting and Sizing Nanoparticles via Single Particle Inductively Coupled Plasma Mass Spectrometry, *Anal. Chem.*, 2011, **83**, 9361–9369.
- 39 M. Tanner and D. Günther, Short transient signals, a challenge for inductively coupled plasma mass spectrometry, a review, *Anal. Chim. Acta*, 2009, **633**, 19–28.
- 40 L. A. Currie, Limits for qualitative detection and quantitative determination. Application to radiochemistry, *Anal. Chem.*, 1968, **40**, 586–593.
- 41 L. A. Currie, Nomenclature in evaluation of analytical methods including detection and quantification capabilities (IUPAC Recommendations 1995), *Pure Appl. Chem.*, 1995, **67**, 1699–1723.
- 42 A. Gundlach-Graham and R. Lancaster, Mass-Dependent Critical Value Expressions for Particle Finding in Single-Particle ICP-TOFMS, *Anal. Chem.*, 2023, **95**, 5618–5626.
- 43 P. A. Freedman and K. Newman, Detection arrangements in mass spectrometers, *US Pat.*, 8084751, 2011.
- 44 J. W. Olesik, J. A. Hartshorne, N. Casey, E. Linard and J. R. Dettman, Further insight into analyte transport



- processes and water vapor, aerosol loading in ICP-OES and ICP-MS, *Spectrochim. Acta, Part B*, 2021, **176**, 106038.
- 45 S. G. Bevers, C. Smith, S. Brown, N. Malone, D. H. Fairbrother, A. J. Goodman and J. F. Ranville, Improved methodology for the analysis of polydisperse engineered and natural colloids by single particle inductively coupled plasma mass spectrometry (spICP-MS), *Environ. Sci.: Nano*, 2023, **10**, 3136–3148.
  - 46 K.-S. Ho, K.-O. Lui, K.-H. Lee and W.-T. Chan, Considerations of particle vaporization and analyte diffusion in single-particle inductively coupled plasma-mass spectrometry, *Spectrochim. Acta, Part B*, 2013, **89**, 30–39.
  - 47 A. Laycock, N. J. Clark, R. Clough, R. Smith and R. D. Handy, Determination of metallic nanoparticles in biological samples by single particle ICP-MS: a systematic review from sample collection to analysis, *Environ. Sci.: Nano*, 2022, **9**, 420–453.
  - 48 D. Ojeda, E. Bolea, J. Pérez-Arantegui and F. Laborda, Exploring the boundaries in the analysis of large particles by single particle inductively coupled plasma mass spectrometry: application to nanoclays, *J. Anal. At. Spectrom.*, 2022, **37**, 1501–1511.
  - 49 J. Liu, K. E. Murphy, R. I. Maccuspie and M. R. Winchester, Capabilities of Single Particle Inductively Coupled Plasma Mass Spectrometry for the Size Measurement of Nanoparticles: A Case Study on Gold Nanoparticles, *Anal. Chem.*, 2014, **86**, 3405–3414.
  - 50 S. Yamashita, M. Nakazato and T. Hirata, Size Analysis of Small Metal Nanoparticles Using Single Particle ICP Mass Spectrometry, *Anal. Sci.*, 2021, **37**, 1637–1640.
  - 51 C. Degueldre, P. Y. Favarger and S. Wold, Gold colloid analysis by inductively coupled plasma-mass spectrometry in a single particle mode, *Anal. Chim. Acta*, 2006, **555**, 263–268.
  - 52 I. Strengé and C. Engelhard, Single particle inductively coupled plasma mass spectrometry: investigating nonlinear response observed in pulse counting mode and extending the linear dynamic range by compensating for dead time related count losses on a microsecond timescale, *J. Anal. At. Spectrom.*, 2020, **35**, 84–99.
  - 53 S. Yamashita, A. Miyake and T. Hirata, Size analysis of large-sized gold nanoparticles using single particle ICP-mass spectrometry, *J. Anal. At. Spectrom.*, 2020, **35**, 2834–2839.
  - 54 TechNote 104 Silica Microspheres, Bangs Laboratories, Inc., 2013, [https://bangslabs.com/wp-content/uploads/BLI\\_TN104\\_SilicsMicrospheres.pdf](https://bangslabs.com/wp-content/uploads/BLI_TN104_SilicsMicrospheres.pdf).
  - 55 A. C. Gimenez-Ingalaturre, K. Ben-Jeddou, J. Perez-Arantegui, M. S. Jimenez, E. Bolea and F. Laborda, How to trust size distributions obtained by single particle inductively coupled plasma mass spectrometry analysis, *Anal. Bioanal. Chem.*, 2023, **415**, 2101–2112.
  - 56 P. Warburton, A. Donard, L. Schlatt, P. Shaw and J. Cottle, *Presented in Part at the Goldschmidt*, 2023.

